

PAPER

## Understanding quench in no-insulation (NI) REBCO magnets through experiments and simulations

To cite this article: Kabindra R Bhattarai *et al* 2020 *Supercond. Sci. Technol.* **33** 035002

View the [article online](#) for updates and enhancements.



**IOP | ebooks™**

Bringing together innovative digital publishing with leading authors from the global scientific community.

Start exploring the collection—download the first chapter of every title for free.

# Understanding quench in no-insulation (NI) REBCO magnets through experiments and simulations

Kabindra R Bhattarai<sup>1</sup>, Kwanglok Kim<sup>1</sup>, Kwangmin Kim<sup>1</sup>, Kyle Radcliff<sup>1</sup>, Xinbo Hu<sup>1</sup>, Chaemin Im<sup>2</sup> , Thomas Painter<sup>1</sup>, Iain Dixon<sup>1</sup>, David Larbalestier<sup>1</sup>, SangGap Lee<sup>3</sup> and Seungyong Hahn<sup>2</sup> 

<sup>1</sup>National High Magnetic Field Laboratory, 1800 East Paul Dirac Drive, Tallahassee, FL 32304, United States of America

<sup>2</sup>Seoul National University, 1 Gwanak-ro, Gwanak-gu, Seoul, Republic of Korea

<sup>3</sup>Korea Basic Science Institute, Daejeon 169-148, Republic of Korea

E-mail: [hahnsy@snu.ac.kr](mailto:hahnsy@snu.ac.kr)

Received 10 September 2019, revised 8 December 2019

Accepted for publication 31 December 2019

Published 27 January 2020



CrossMark

## Abstract

Present research on no-insulation (NI) rare earth barium copper oxide (REBCO) magnets have demonstrated their ability to produce high fields due to their compact nature. NI magnets have often been demonstrated to be self-protecting. However, evidence of mechanical damage in recent high field magnets, suggests that there are some issues about quench that must be resolved for this otherwise promising technology. This article attempts to explain multi-physics phenomena occurring during the quench of an NI magnet that can be used to elucidate quench behavior through experiments and simulations. A *lumped circuit model* is used for the circuit analysis where each coil is modeled as a single inductor with variable quench resistance in series and characteristic contact resistance in parallel. Three case studies have been analyzed: (1) a 3 double pancake (DP) standalone magnet, (2) a 2 DP coil in 31 T background, and (3) a high temperature superconductor/low temperature superconductor (HTS/LTS) hybrid user magnet that consists of a 13 T HTS insert and a 6 T LTS background magnet. Lessons learned from these analyses include: (1) characteristic resistance of NI coil rises during quench with the temperature rise; (2) influence of Hall effect exists on the voltage rise during quench; (3) over-current during quench can over-stress the coil; and (4) quench propagation from one end of the magnet generates significant unbalanced forces. This approach is expected to be used in the preliminary design of an ultra high field (>40 T) user magnet currently under design at the National High Magnetic Field Laboratory.

Keywords: HTS magnet, no-insulation, protection, quench, simulation

(Some figures may appear in colour only in the online journal)

## 1. Introduction

Since the multi-width (MW) no-insulation (NI) winding technique was introduced [1, 2], a number of insert coils and standalone magnets have been designed and constructed using this method, focusing on applications including nuclear magnetic resonance (NMR) and high field generation. Due to the absence of insulation in this technique, the magnet becomes compact and mechanically robust making it a

suitable candidate for ultra-high field magnets. The absence of insulation allows *current sharing*, which can make an NI magnet essentially free from electrical burning. Y S Choi *et al* proposed a 5 T high temperature superconductor (HTS) insert for NMR applications [3] and later a 4 T standalone cryo-cooled magnet was successfully constructed and tested [4]. In the upcoming years, 7 T [5] and 26 T [6] standalone magnets were constructed, tested for high field generation and they also demonstrated survival even after multiple over-current

quenches. Similarly, NI HTS inserts in low temperature superconductor (LTS) outserts were also demonstrated for the generation of fields greater than or equal to 20 T [7–9]. Park *et al* constructed and tested a nested configuration of NI rare earth barium copper oxide (REBCO) for GHz class NMR [10]. ‘Metal as insulation’ variant of no-insulation winding, also known as ‘stainless steel clad’ magnets, have also been constructed and tested [11, 12], reducing charging delay. Suetomi *et al* tested a no-insulation layer wound version of the winding method [13] which could prove promising in the future. Interest shown by Scheidler and Talerico at NASA [14] and industrial applications such as an induction heater by Supercoil Co. Ltd. [15] have demonstrated the large potential for NI technology outside of high field generation as well. Recent reports have shown the potential of NI magnets in the generation of ultra-high fields, and at the same time, have shown that this technology is not completely devoid of possibilities for mechanical damage [16]. We believe that there is a need to learn from these damages and understand the multiphysics behind the quenches to design truly reliable future high field magnets.

The first simulation of the charging behavior of an NI HTS magnet used an equivalent circuit model that consisted of an inductor and a resistor connected in parallel [1]. Significant progress has been made by researchers since then in the numerical simulation of NI magnets. Wang *et al* investigated the turn-to-turn contact characteristics of an NI coil and refined the lumped circuit model in combination with the  $n$ -value index model [17]. We earlier reported a ‘magnet-level’ lumped circuit quench simulation of a 7 T 78 mm all-REBCO NI magnet that was designed, constructed, and operated at MIT [18]. Yang *et al* [19] also reported a similar lumped-circuit analysis. The lumped-circuit model enables fast simulation with reasonable accuracy of the transient electromechanical behavior of an NI magnet. Yanagisawa *et al* at RIKEN were the first group to do quench simulations with a distributed model at the coil level [20] and later Markiewicz *et al* at the National High Magnetic Field Laboratory (NHMFL) [21] and Song *et al* [22] came out with the first magnet level simulations. Researchers around the world have conducted detailed simulations based on the distributed approach at the single coil level [23–28] and the full magnet level [29]. However, the distributed model simulation of an ‘actual’ NI HTS magnet has not been performed yet; the long calculation time, often over a week or even a month for simulation of a single operational scenario, may be the primary obstacle for the distributed model to be more commonly adopted given that there are many poorly defined physical properties of HTS conductors with significant uncertainty that must be modeled. Since we have been designing and building many test magnets we needed more rapid methods to explore the self-protection mechanism at the magnet level under various charging and quenching scenarios. Our goal was to identify the limits of safe NI magnet performance through comparison of experimental and simulation results. Therefore, in this research project, we use the lumped circuit approach to calculate currents, voltages, temperatures, magnetic fields, and mechanical stresses. Note that some simulated

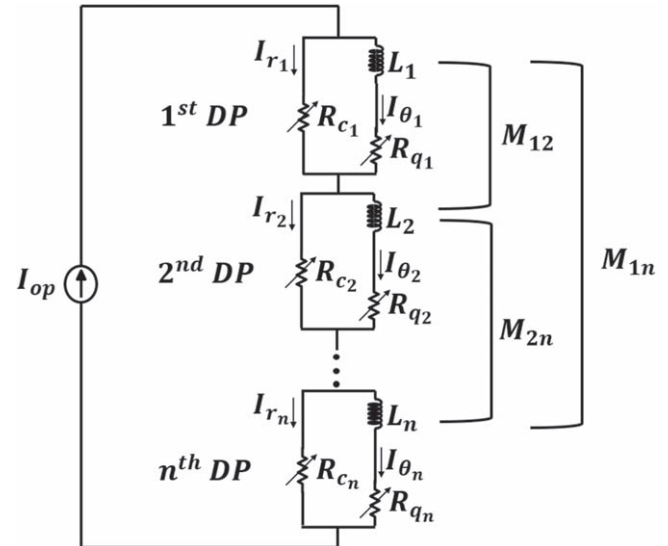


**Figure 1.** Lumped circuit model of a stack of no-insulation magnet with ‘ $n$ ’ number of pancake coils.

parameters, including radial current, temperature, and radial and hoop stress of individual pancake coils (PCs) are difficult to measure during quench.

## 2. Method of quench analysis

The quench analysis is a multi-physics problem. The modeling included circuit and thermal analyses done using the lumped-parameter approach [18]. In this approach, each of the subcoils are described by lumped parameters, including inductance, resistance and temperature, and consequent equivalent circuit of a series connected magnet is modeled as shown in figure 1. The model has been further expanded to include electromechanical stress analysis. The necessary governing equations are formulated using the methods described below, are then discretized, and numerically solved using an in house MATLAB code. The coupled circuit, thermal, magnetic and mechanical stress analyses are described in the following subsections.

### 2.1. Circuit analysis

The circuit analysis is done to solve for the time-varying current,  $I(t)$  and voltage,  $V(t)$  at each of the subcoils. The circuit analysis can be broken down into three items.

- Lumped circuit model and solution of Kirchoff’s equations:

In the lumped-circuit model of an NI coil, treating a pancake coil as a single entity is assumed to be valid provided that quench propagation happens electromagnetically and thus almost simultaneously across a single pancake, in contrast to the slow thermal quench propagation of conventional insulated coils. This method models a single pancake as a single inductor,  $L$  with mutual coupling,  $M$  with other coils, a single

characteristic contact resistance,  $R_c$  and an azimuthal quench resistance,  $R_q$ . The self inductance and mutual inductance of the coils are solved using elliptic integral and Gaussian numerical quadrature as described by Garrett [30].  $R_{ct}$  represents an average turn-to-turn contact resistance that can be directly estimated by a simple charging test [17]. The characteristic resistance of the NI coil,  $R_c$  is obtained from equation (1) where  $r_i$  and  $w_d$ , respectively, are the radius of the  $i^{th}$  turn and the width of the HTS tape used to wind the coil with  $N_t$  turns.

$$R_c = \sum_{i=1}^{N_t} \frac{R_{ct}}{2\pi r_i w_d} \quad (1)$$

From Kirchoff's voltage law for 'n' number of loops in the circuit shown in figure 1 gives 'n' number of equations. The equations are numerically solved using finite difference method.

- Modeling of azimuthal quench resistance,  $R_q$ .

The quench resistance,  $R_q$  is equivalent resistance given by resistance across the superconductor,  $R_{sc}$  and across the stabilizer,  $R_s$ . The resistance across the superconductor is calculated using the well known power law, equation (2), that explains the non-linear behavior of HTS tapes. Here,  $V_c$  is the critical voltage given by the  $1 \mu\text{V}/\text{cm}$  criterion.  $I_c(B(t), \theta(t))$  is the field and angle dependent critical current.  $n$  is the index value of the superconductor for which a typical value of 30 is used for this simulation [31] and  $I_{sc}$  is the current flowing through the superconductor.

$$R_{sc}(t) = \frac{V_c}{I_{sc}(t)} \left( \frac{I_{sc}}{I_c(B(t), \theta(t))} \right)^n \quad (2)$$

- Modeling of critical current,  $I_c$ :

Field and angular dependencies of the critical current are incorporated with the empirical function presented by Hilton *et al* [32]. The reduction of critical current with the temperature is also incorporated, using a  $T^*$  value of 15 [33] as given in equation (3), where  $J_c$  is the critical current density. The  $T^*$  value of 15 indicates that the critical current drops by half when there is a temperature rise of 10 K.

$$J_c(T, B) = J_c(T = 0, B) e^{-T/T^*} \quad (3)$$

## 2.2. Thermal analysis

The thermal analysis model finds the time-varying average temperature  $T(t)$  of an individual pancake coil due to resistive joule heating. The governing equation for heat transfer is given by equation (4). Here,  $\rho$ ,  $C_p$ ,  $\dot{q}$ ,  $k$ ,  $h$ ,  $P$ ,  $A$ , and  $T_\infty$  represent, respectively, density, heat capacity, joule heating, thermal conductivity, film coefficient, perimeter exposed to cryogen, cross sectional area of coil and temperature of the bath. The second and third terms on the right-hand side stand for heat conduction within the coil and convective transfer into the cryogen, respectively. The disturbance energy is often

neglected in simulation of an HTS magnet quench, mainly due to the large stability margin of HTS [34]. The thermal analysis and circuit analysis are coupled as  $I_c$  depends on temperature and Joule heating depends on operating current. As the quench propagation in an NI coil is rapid and electromagnetic, the stored magnetic energy may be assumed to be dissipated evenly over the whole volume of the magnet. This might be a rather strong assumption, which may further need to be verified experimentally. However, simulation work by Markiewicz *et al* [21] shows the variation of temperature across pancake is very small compared to the rise in the temperature during quench. Experimental fluorescent thermal imaging by Gyuraki *et al* shows that hot spot is not concentrated around the local point defect, but warmer regions of relatively uniform temperature spanning a few turns exist near the local defect [35]. The maximum temperature was only about 22 K higher than the initial temperature of the coil. Hence, we use a lumped-capacitance thermal model, where the thermal conduction across the coil, i.e. the second term on the right hand side of the equation (4) is ignored. Also, as the heat generation rate due to joule heating is much higher than the heat dissipation rate due to liquid helium boiling, it is assumed that all of the heat generated is used to raise the temperature of the coil and the last term on equation (4) is ignored as well.

$$\rho C_p(T) \frac{dT}{dt} = \dot{q} + k(T) \nabla^2 T + h(T)(T - T_\infty) \frac{P}{A} \quad (4)$$

The pancakes in NI magnets are electrically isolated using spacers which are also better thermal insulators than metals. NI magnet quenches are very fast, not allowing enough time for significant thermal diffusion between the pancakes. Because of this reason, even though each of the pancakes are lumped thermally, they are thermally isolated from each other in the model.

## 2.3. Magnetic field analysis

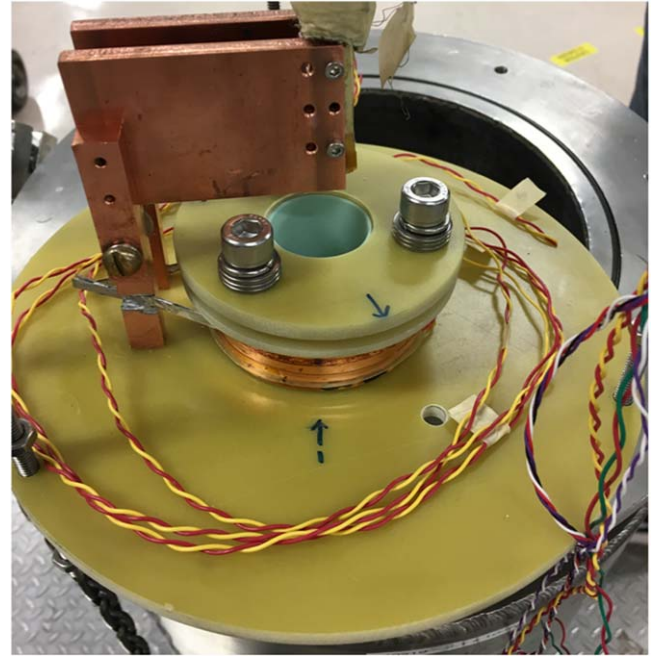
The time varying magnetic field,  $B(t)$  must be calculated as the quench progresses, as  $B(t)$  depends on the changing coil azimuthal current. The elliptic integral based on the Gaussian numerical quadrature method was used to calculate  $B(t)$  [30]. Since we adopted the lumped circuit model, the current density in each pancake coil is assumed to be spatially uniform. Magnetic fields from the radial component are ignored; due to the symmetry of the radial current distribution in the lumped circuit model, the contribution to  $B(t)$  by the radial current is assumed to be zero. Experimentally, this may not be true, due to the asymmetric nature of the radial current distribution.

## 2.4. Mechanical stress/strain analysis

We use the approach of Bovrov and Williams [36] for our mechanical stress analysis. Assuming that the mechanical stress of a solenoid magnet is at its peak on the magnet's midplane, the force balance equation (5) is adopted as the governing equation for our stress analysis, where  $r$ ,  $\sigma_r$ ,  $\sigma_\theta$ ,  $J_\theta$ ,

**Table 1.** Key Parameters of the 4.72 T, 40 mm Magnet.

Parameter	Units	Value
<b>Conductor Parameters</b>		
Manufacturer		SuNAM
Average tape width	mm	4.1
Tape thickness	$\mu\text{m}$	115
Copper stabilizer thickness	$\mu\text{m}$	15 (7.5/side)
<b>Configuration</b>		
Coil i.d.; o.d.	mm	40; 78.9
Turns per pancake		169
Overall height	mm	25.6
Number of DP		3
<b>Operation</b>		
Temperature, $T$	K	4.2
Quench current, $I_\theta$	A	243
Inductance	mH	47.7
Stored energy	kJ	1.4
Characteristic resistance, $R_c$	$\text{m}\Omega$	0.97
Charging time constant, $\tau_c$	min	49.18
Magnet constant	$\text{mT/A}$	20.1

**Figure 2.** 40 mm winding diameter magnet with a stack of 3 double pancakes that was charged up to 243 A in liquid helium (with corresponding center field of 4.72 T) and was then quenched. The key parameters are summarized in table 1.

and  $B_z$  are, respectively the radius, radial stress, hoop stress, azimuthal current density and axial field. The self-supporting turn effect, i.e.,  $\sigma_r = 0$ , of a dry winding is also considered in our simulation as a boundary condition. Using the generalized Hooke's law, magnetic strain on the magnet is calculated. Anisotropic elastic properties of the 'composite' winding of the magnet were calculated using the rule of mixtures. In addition to magnetic strain, bending strain during winding was also calculated to obtain the final strain.

$$r \frac{\partial \sigma_r}{\partial r} + \sigma_r - \sigma_\theta + r J_\theta B_z(r) = 0 \quad (5)$$

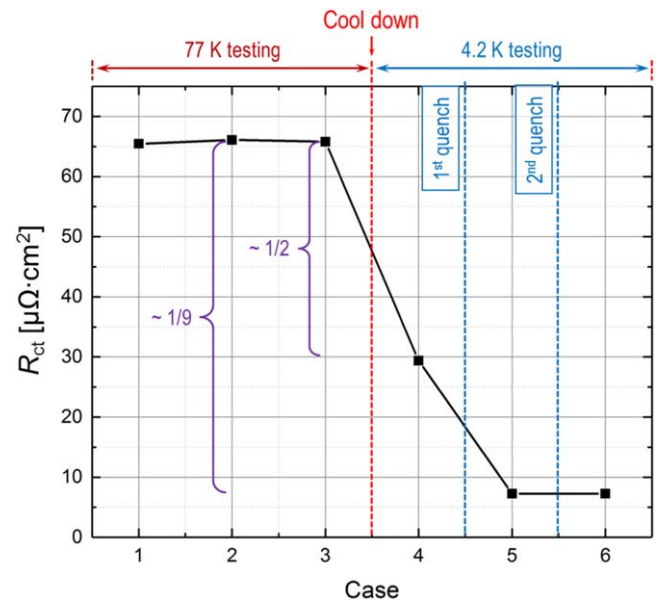
### 3. Quench analysis of 3 magnets and lessons learned

#### 3.1. Evidence of rise in characteristic resistance due to temperature rise

The first magnet in consideration is a 3-double-pancake magnet that used REBCO tape of 4.1 mm width. The key parameters are summarized in table 1.

During winding, the REBCO layer was faced radially inward, so that the superconductor layer experiences a compressive bending strain that, in turn lowers the overall peak strain. The double pancakes were then stacked and connected in series to produce the magnet shown in figure 2. Signals for voltage, current and magnet center field were monitored with a National Instrument's LABVIEW data acquisition system.

The magnet was cooled down to 4.2 K in a bath of liquid helium. First, ramp up and ramp down tests were done to estimate the characteristic resistance,  $R_c$ . Second, the magnet

**Figure 3.** Contact resistance,  $R_{ct}$  decreased as the magnet was cooled down from 77 K (Case 1-3) to 4.2 K (Case 4) by a factor of 1/2. After quench at 4.2 K, it decreased even further by a factor of 1/9 compared to the value at 77 K (Cases 5 and 6).

was ramped up until it quenched at 243 A, which corresponds to a center field of 4.72 T.

The contact resistance of the magnet changes as the magnet is cooled down from 77 K to 4.2 K as seen in figure 3. This shows that  $R_{ct}$  is influenced by the temperature of the coil. This is probably because  $R_{ct}$  depends on the resistivity of the Cu contact surface material.

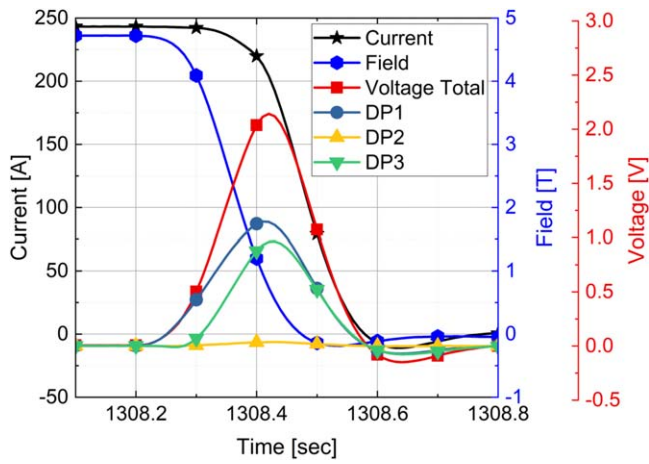
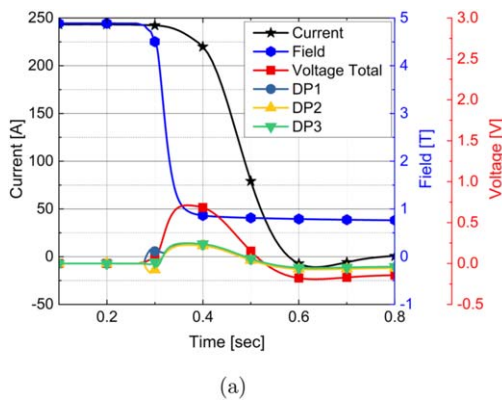


**Figure 4.** Experimental data showing the coil terminal voltages, magnetic center fields, and power supply currents of the magnet during quench.

The experimental high resolution quench data are presented in figure 4. They show very fast quench propagation and fast discharge of the magnetic field, indicating quench propagation to all three double pancakes.

Various time-varying parameters calculated by the simulation model such as current, voltage and temperature during the quench have been described below. Using the measured current in the shunt resistor placed between the power supply and the magnet, the power supply was modeled as an independent current source in our simulation.

Simulation of the coil voltage (figure 5(a)) showed that the voltage of the topmost DP started rising first, indicating that the quench started from DP1. When DP1 quenched, the voltage of the adjacent coils first reduced, due to the interaction among magnetically coupled coils for flux conservation [34], then started to rise when the other coils quenched. Even though the simulated and experimental voltages have a similar pattern, the differences between them cannot be ignored. As seen in figure 3, we believe that  $R_c$  increases during the temperature rise of quench. This idea was also proposed by Lu *et al* [37]. Hence the simulation was updated to let the value of  $R_c$  increase proportionally to the  $\rho(T)$  of the Cu stabilizer as given by equation (6). The updated results are



(a)

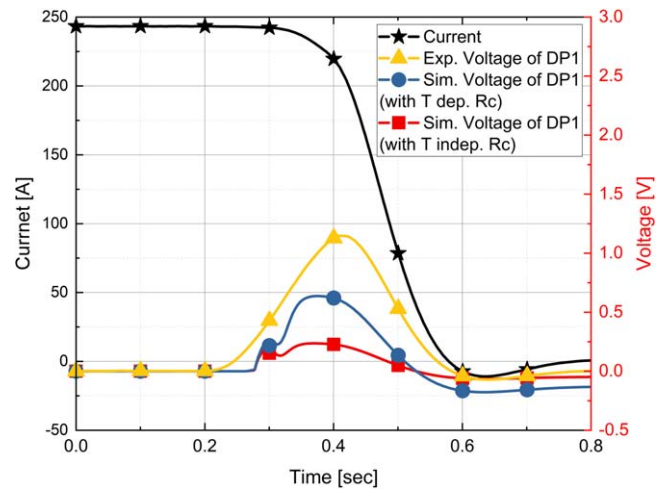
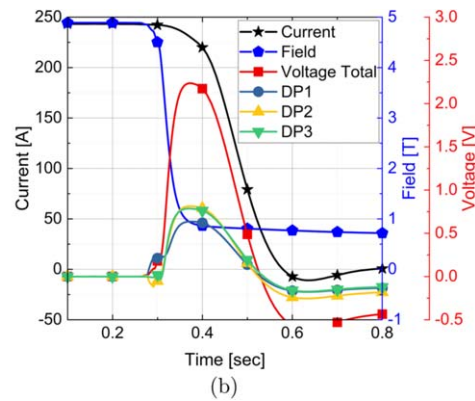


**Figure 6.** Graph of voltage across DP1 of the 3-DP coil. (i) experimentally measured voltage (orange triangles), (ii) simulated voltage without temperature dependency on  $R_c$  (red circles) and (iii) simulated voltage with temperature dependency on  $R_c(T)$  (blue circles). Here black stars indicate the power supply current.

shown in figure 5(b) and a comparison of experiment and simulations for DP1 are shown in figure 6. They show that the model now has much better simulation of both the voltage behavior and voltage values demonstrated by the experiment, but some degree of error still persists. Quench modeling involves multiphysical parameters, with some of them having varying degree of uncertainties, particularly the critical current of the conductor and the turn-to-turn contact resistance. Despite best simulation efforts, some differences between the experiments and simulations are inevitable.

$$R_c(T) = R_c(4.2K) \frac{\rho_{cu}(T)}{\rho_{cu}(4.2K)} \quad (6)$$

In the simulation,  $R_c$  increases by about 3 times with the temperature as seen in figure 7. This simulated rise in  $R_c$  is due to its coupling with the thermal model as described in equation (6). The heat generated in the coil due to Joule heating increases the temperature of the coil as seen in figure 8. The final average temperature of the coil was calculated to be 55.2 K. We do make an adiabatic assumption



(b)

**Figure 5.** (a) Simulated voltages of the 3-DP coil without temperature dependency on  $R_c$ . Stars stand for power supply current, hexagons for magnetic center fields, circles, triangles and inverted triangles for the respective simulated voltage values of DP1, DP2 and DP3, square for the overall magnet terminal voltage. (b) Simulated voltage of 3-DP coil after the  $R_c(T)$  was made temperature dependent.

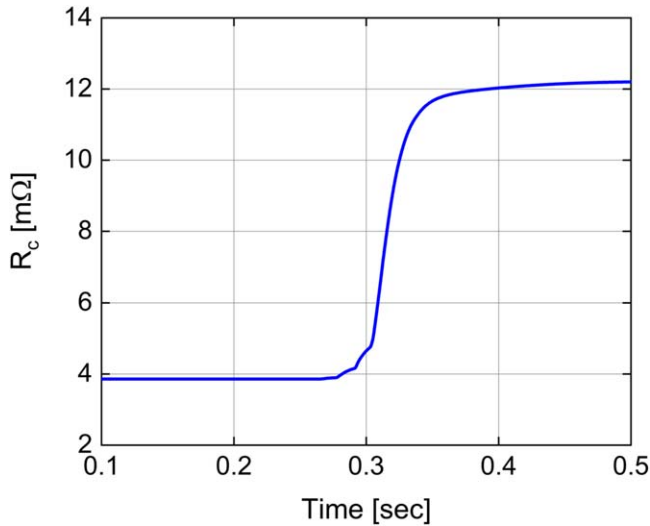


**Figure 7.** Simulated  $R_c$  shows 3-fold rise in  $R_c$  value during quench as temperature rises from 4.2 K to 55.2 K.

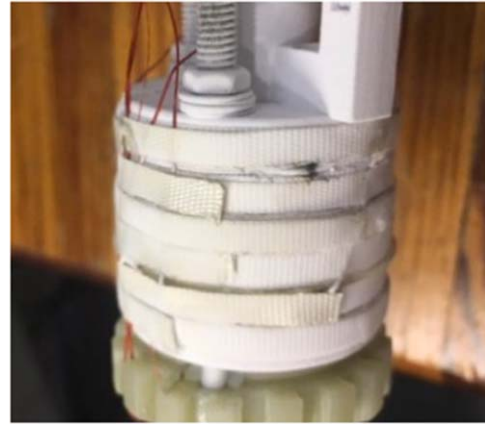


**Figure 9.** 14 mm bore magnet with a stack of 2 DP REBCO coils operated in 31 T.

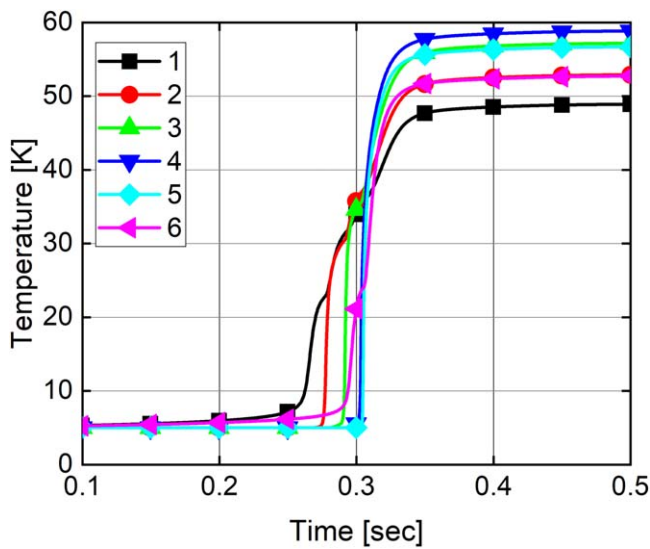


**Figure 8.** Temperature rise during quench due to Joule heating as stored energy converts to thermal energy.

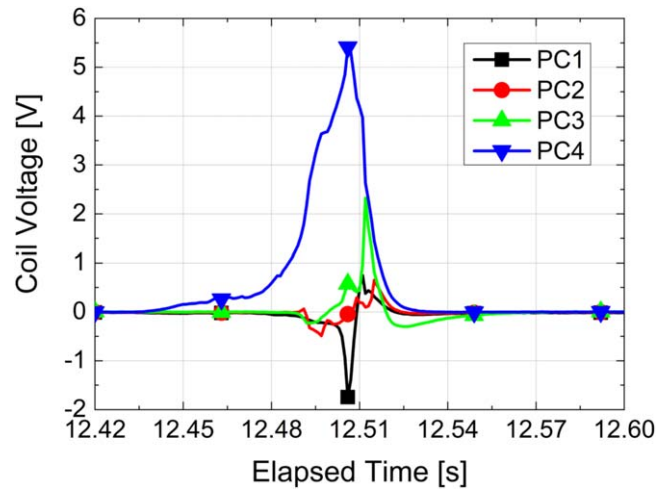


**Figure 10.** Experimentally measured voltage data across each of the pancakes that form the 2 DP coil, with respect to time during quench.

and there is consequent potential to overestimate the peak temperature, making this a safer and more conservative estimate of the peak coil temperature.

Initially stored 1370 J of magnetic energy in the coil changed to heat during the complete quench. The energy balance of this phenomenon is given by equation (7). Here the left hand side of the equation gives the stored magnetic

**Table 2.** Key Parameters of the 2 DP Coil in 31 T Background.

Parameter	Units	Value
<b>Conductor</b>		
Manufacturer		SuperPower
Tape width; Thickness	mm	4.03; 0.045
Cu stabilizer thickness	$\mu\text{m}$	10 (5/side)
<b>NI Insert Configuration</b>		
Coil i.d.; o.d.	mm	14; 34
Turns per DP		430
Overall height	mm	16.48
Temperature, $T$	K	4.2
Quench current, $I_\theta$	A	210
Inductance	mH	11
Characteristic resistance, $R_c$	$\text{m}\Omega$	2.4
Charging time constant, $\tau_c$	sec	4.58
Magnet constant	$\text{mT/A}$	38.7
<b>Background</b>		
Field due to background	T	31.2

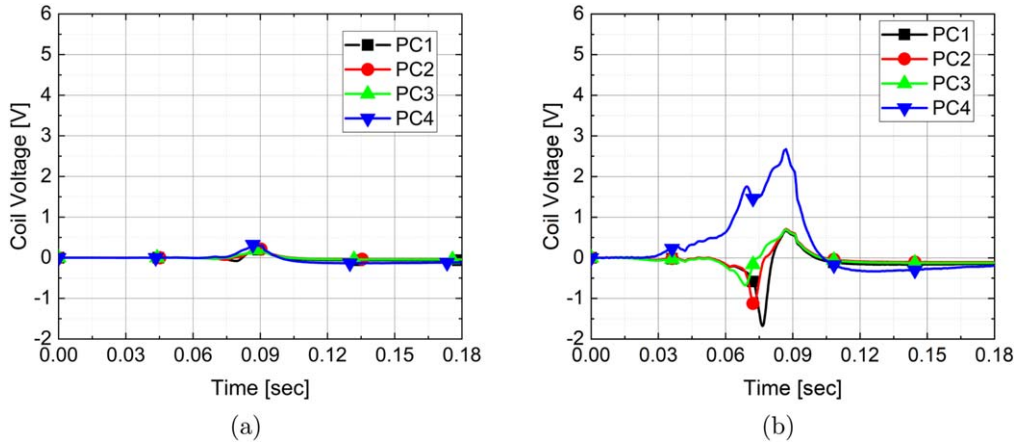


**Figure 11.** Simulation of voltage across each of the 4 pancakes of the 2-DP coil quench (a) without the Hall Effect and (b) with Hall effect taken into consideration.

energy and  $m$  represents the mass of magnet.

$$\frac{1}{2}LI^2 = \int_{4.2K}^{T_2} mC_p(T)dT \quad (7)$$

Some discrepancy between the simulation and experiment occurred particularly in the simulated magnetic field after the quench. The fast discharge of magnetic field is seen in both experiment and simulation in figure 4 and figure 5(b) respectively. This indicates that the quench has propagated to all coils. However, the simulated field does not discharge completely while it does in the experiment.

### 3.2. Indication of influence of the Hall effect on voltage rise during quench

The second magnet in consideration is a stack of a 2 DP NI coils made out of REBCO tape manufactured by SuperPower Inc. as shown in figure 9. This coil was operated in a 31 T background field generated by a resistive magnet. The key parameters of the coils are described in table 2. In this case too the REBCO layer faced inwards. The magnet was operated in liquid helium and quenched at 210 A. We did similar quench analysis in this case as we did for the previous magnet. This time we learned a new lesson as described below.

The experimentally obtained quench data are shown in figure 10. Quench simulation was done using the same methods described above, now including a rise in  $R_c$  due to the coil temperature rise. The simulated voltage values are shown in figure 11(a). However, the magnitude of the voltage observed in simulation is much smaller—almost negligible—compared to the experiment.

When the current density and the magnetic field are both high, the current flowing through the radial path can be influenced by the Hall Effect, as proposed by Noguchi *et al* [38]. This could be why the experimentally measured voltage is larger than the simulated one in this case. The influence of the Hall Effect is given by equation (8) where  $V_h$  and  $R_h$  indicate the Hall voltage and Hall constant of the material respectively.  $R_h$  value of  $0.55 \times 10^{-10} \text{ m}^3/\text{C}$  is used in the simulation. When this effect is incorporated into the

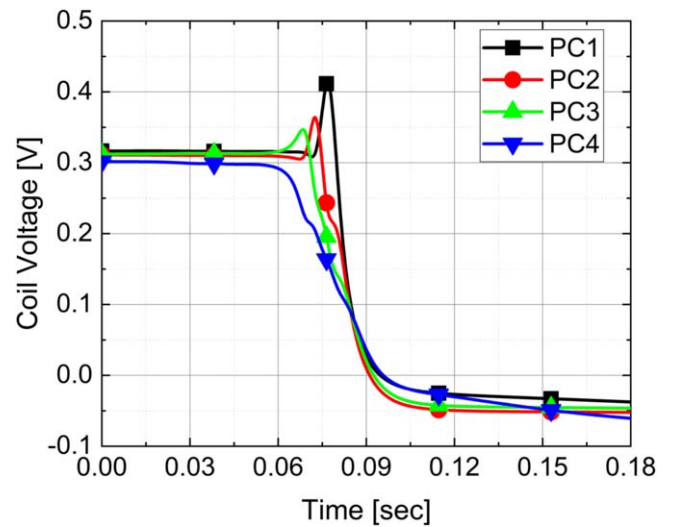


**Figure 12.** Simulated maximum mechanical strain on the REBCO layer for each of the pancakes during quench of 2 DP coil.

simulation, the voltage becomes comparable to the experimental voltage as seen in figure 11(b).

$$V_h = -R_h(J \times B) \quad (8)$$

### 3.3. Possibility of over-stress due to over-current during quench propagation

In this same 2 DP magnet operated in 31 T background field, quench initiated in one pancake, causes the current in the adjacent coil to increase until it reaches its  $I_c$  due to strong inductive coupling between the pancakes. During this type of cascading electromagnetic quench propagation, large over-currents induced can produce large strain in the superconductor layer, as shown in figure 12. This phenomenon becomes particularly important in presence of large background field. This over-strain can damage the superconductor if it strains the tape beyond its irreversible strain limit.

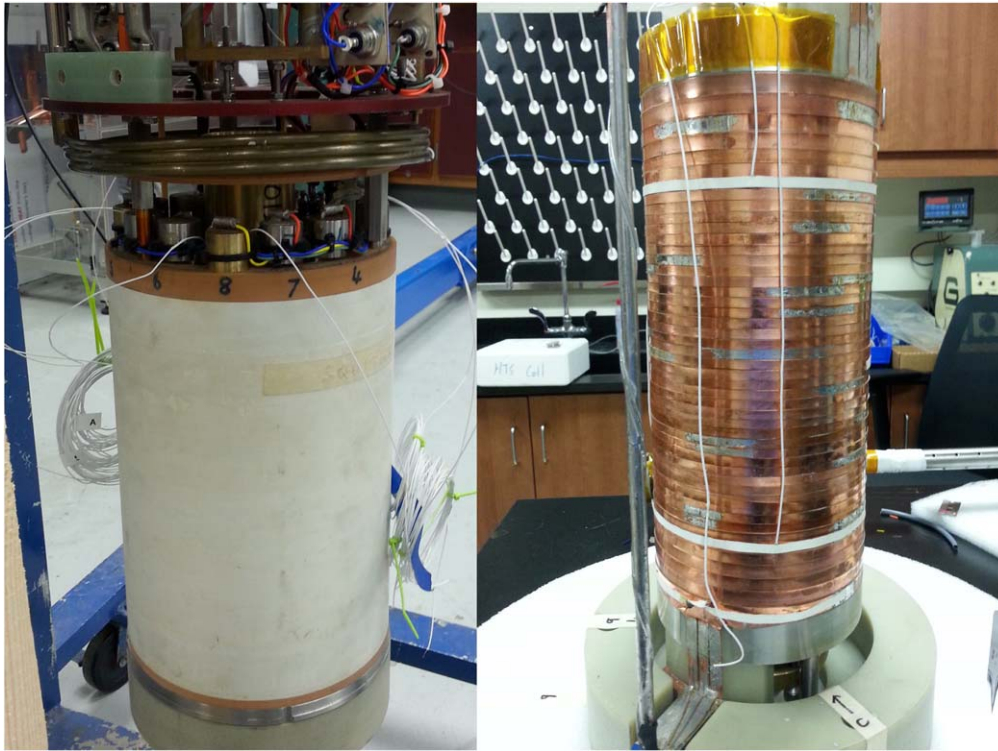


**Figure 13.** 13 T NI REBCO insert (right) in NbTi LTS outsert magnet (left) [8].

**Table 3.** Key Parameters of the 20 T LTS/HTS magnet.

Parameter	Units	Value
<b>Conductor</b>		
Manufacturer.		SuNAM
Tape width; Thickness	mm	4.1-7.1; 0.12
Cu stabilizer thickness	$\mu\text{m}$	20 (10/side)
<b>NI Insert Configuration</b>		
Coil i.d.; o.d.	mm	58; 114
Turns per DP		460
Overall height	mm	233
Quench current, $I_\theta$	A	216
Temperature, $T$	K	4.2
Inductance	H	2.82
Characteristic resistance, $R_c$	$\text{m}\Omega$	50.3
Charging time constant, $\tau_c$	sec	26.2
Magnet constant	$\text{mT/A}$	61.03
<b>Background</b>		
Field due of the background	T	6

### 3.4. Significant magnetic centering forces during quench propagation from one end

This third magnet, named 20 T LTS/HTS magnet, is a stack of 24-DP NI coils made out of REBCO tape manufactured by SuNAM which was operated in a Nb-Ti outsert magnet as shown in figure 13 [8]. The key parameters of the conductor and the magnet are described in table 3. In this case also the REBCO layer faced inwards. The magnet was operated in liquid helium. While the magnet center field was 19 T, and HTS magnet was operating at 216 A, the LTS background

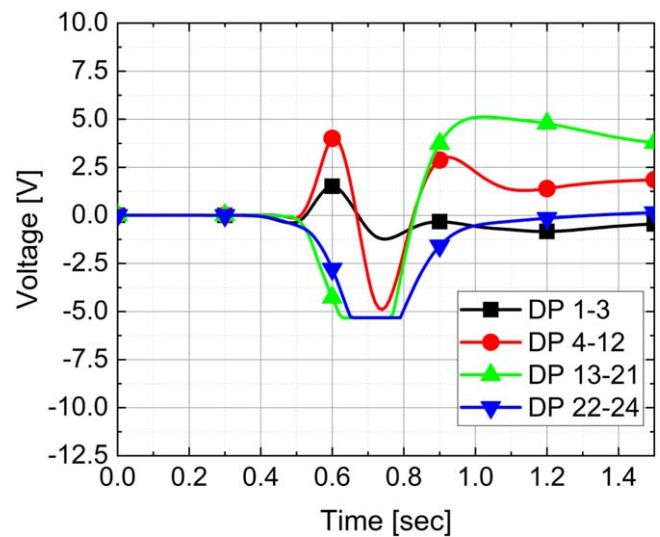


**Figure 14.** Experimentally obtained voltage across each of the 4 modules of 13 T insert quench in 6 T background. The electromagnetic quench propagation happens from one axial end of the magnet to the other. Note that voltage signals from DP13-21 and DP22-24 were not obtained throughout the quench propagation due to the saturation of data acquisition at  $-5$  V.

magnet was ramping and quenched before reaching full field of 20 T. The lessons learned in the above cases were used to simulate quench in this particular case as well. For voltage measurement, the magnet was divided into four modules. The experimentally measured voltages from 4 modules of the magnet are shown in figure 14 and compared to the simulated voltages in figure 15. Comparison of the two figures shows that the simulated voltage behavior, quench propagation

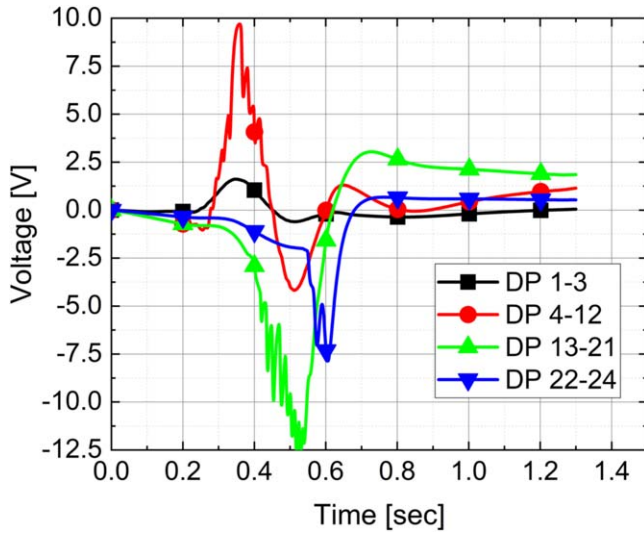


**Figure 15.** Simulation of voltages across each of the 4 modules of 13 T insert quench in 6 T background.

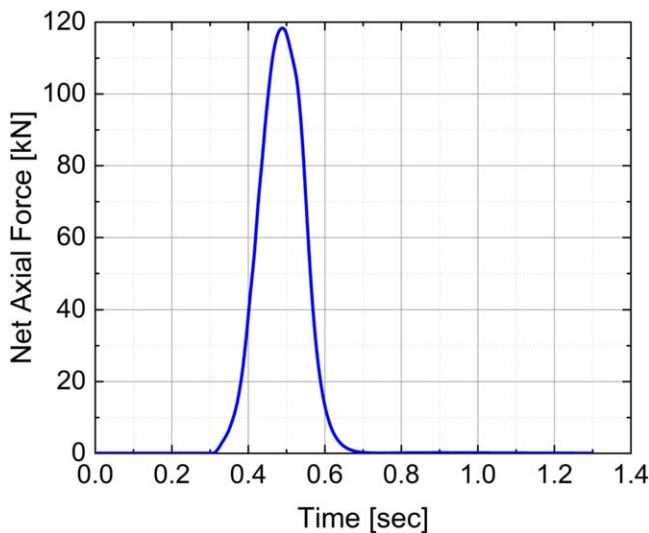


**Figure 16.** Simulated axial force on the 13 T insert magnet showing large centering force generated during quench.

speed and magnitude are similar to those measured during the experiment.

One important lesson was learned in this magnet analysis that was not observed in the previous case studies. Due to the flux conservation during quench, currents are induced unevenly in pancake coils. As a result, the Lorentz's forces in axial direction of the NI insert will no longer balance in the presence of a background field, which in this case is the field produced by the LTS magnet. This force exists due to interaction between the radial magnetic field,  $B_r$  and the azimuthal current density,  $J_\theta$  producing forces in axial direction,  $F_z$  given by equation (9), where  $V$  is the volume of a pancake

coil.

$$\mathbf{F}_z = \int_V \mathbf{J}_\theta \times \mathbf{B}_r \quad (9)$$

The simulation showed that this force can be as high as 119 kN during quench propagation, as shown in figure 16. In this particular case, this force damaged the support structures that kept the two nested magnets centered. Similar structural damage in nested configuration was also reported by another research group [39–41].

#### 4. Conclusion

Comparison of experiments and simulations of NI quenches have provided important insights into the dynamics of quench in NI magnets. The important lessons learned can be summarized as:

- The NI characteristic resistance,  $R_c$  is not constant during a quench and increases with the rise in the temperature. This rise in fact follows the  $\rho(T)$  of copper reasonably well.
- When the current density is high and in the presence of a large background field, the characteristic resistance,  $R_c$  is further influenced by the Hall effect.
- The rapid inductive quench propagation and consequent over-currents have the possibility to over-strain the magnet conductor.
- Nested configurations of NI coil inside outserts can make the whole magnet unstable. Quench in such a configuration can produce significant centering forces that can damage the magnet structure.

Despite the inevitable simplicity of our lumped-circuit model, the simulations do represent the essential features of the experimental quench properties. The simulation generated insights on parameters such as temperature, stress and strain that cannot be easily measured during experiments. Our recent experiments have shown that the effect of screening currents on field, stresses and AC losses are important [16], but have not yet been incorporated into this analysis yet. Through experiments and simulations, we have developed a useful understanding of quench behavior in no-insulation magnets. This method, which is computationally less intensive than other methods proposed by other researchers, will help in designing magnets that do not exceed their safe stresses and strains when quenched. This is crucial to making sure that the no-insulation winding technique remains truly reliable even when the magnets quench under high fields.

#### Acknowledgments

This work was funded by the National High Magnetic Field Laboratory (which is supported by the National Science Foundation under NSF/DMR-1644779), the State of Florida, and the Korea Basic Science Institute (KBSI) grant (D39611).

A part of works by S Hahn and C Im was supported by the National Research Foundation of Korea (NRF) grant funded by the Korea government (MSIT) (No. 2018R1A2B3009249).

## ORCID iDs

Chaemin Im  <https://orcid.org/0000-0002-3591-9805>

Seungyong Hahn  <https://orcid.org/0000-0002-4511-4162>

## References

- [1] Hahn S, Park D K, Bascuñán J and Iwasa Y 2011 HTS pancake coils without turn-to-turn insulation *IEEE Trans. Appl. Supercond.* **21** 1592–5
- [2] Hahn S, Kim Y, Park D K, Kim K, Voccio J, Bascuñán J and Iwasa Y 2013 No-insulation multi-width winding technique for high temperature superconducting magnet *Appl. Phys. Lett.* **103** 173511
- [3] Choi Y S, Kim D L and Hahn S 2011 Progress on the development of a 5 T HTS insert magnet for GHz class NMR applications *IEEE Trans. Appl. Supercond.* **21** 1644–8
- [4] Yoon S, Cheon K, Lee H, Moon S, Kim S, Kim Y, Park S, Choi K and Hong G 2014 Fabrication and characterization of 4-T/203 mm RT bore 2G HTS magnet with no-insulation method *IEEE Trans. Appl. Supercond.* **24** 4602904
- [5] Hahn S, Song J, Kim Y, Lecrevisse T, Chu Y, Voccio J, Bascuñán J and Iwasa Y 2015 Construction and test of 7-T/68-mm cold bore multi-width no-insulation GdBCO magnet *IEEE Trans. Appl. Supercond.* **25** 4600405
- [6] Yoon S, Kim J, Cheon K, Lee H, Hahn S and Moon S 2016 26 T 35 mm all-GdBa<sub>2</sub>Cu<sub>3</sub>O<sub>7-x</sub> multi-width no-insulation superconducting magnet *Supercond. Sci. Technol.* **29** 04LT04
- [7] Liu J *et al* 2016 Generation of 24 T with an all superconducting magnet *IEEE/CSC and ESAS Superconductivity News Forum* **10** 35-STH39 <https://snf.ieeeesc.org/abstracts/generation-24-t-all-superconducting-magnet>
- [8] Painter T *et al* 2017 Design, construction and operation of a 13 T 52 mm no insulation REBCO insert for a 20 T all superconducting user magnet *25th International Conf. on Magnet Technology (Amsterdam), Or31-03* <https://indico.cern.ch/event/445667/contributions/2562082/>
- [9] Liu J, Wang L, Qin L, Wang Q and Dai Y 2018 Recent Development of the 25 T All-Superconducting Magnet at IEE *IEEE Trans. Appl. Supercond.* **28** 4301305
- [10] Park D, Bascuñán J, Michael P C, Lee J, Hahn S and Iwasa Y 2018 Construction and test results of coils 2 and 3 of a 3-Nested-Coil 800-MHz REBCO insert for the MIT 1.3-GHz LTS/HTS NMR magnet *IEEE Trans. Appl. Supercond.* **28** 4300205
- [11] Jang J Y, Yoon S, Hahn S, Hwang Y J, Kim J, Shin K H, Cheon K and Kim K 2017 Y.J. Hong, ‘Design, construction and 13 K conduction-cooled operation of a 3 T 100 mm stainless steel cladding all-REBCO magnet’ *Supercond. Sci. Technol.* **30** 105012
- [12] Lécresse T, Badel A, Benkel T, Chaud X, Fazilleau P and Tixador P 2018 Metal-as-insulation variant of no-insulation HTS winding technique: pancake tests under high background magnetic field and high current at 4.2 K *Supercond. Sci. Technol.* **31** 055008
- [13] Suetomi Y, Takahashi S, Takao T, Maeda H and Yanagisawa Y 2019 A novel winding method for a no-insulation layer-wound REBCO coil to provide a short magnetic field delay and self-protect characteristics *Supercond. Sci. Technol.* **32** 045003
- [14] Scheidler J J and Tallerico T F 2018 Design, fabrication, and critical current testing of no-insulation superconducting rotor coils for NASA’s 1.4 MW high-efficiency megawatt motor *AIAA/IEEE Electric Aircraft Technologies Symposium* p 5002
- [15] Choi J, Lee C, Hwang C, Kim S, Cho S, Park M and Yu I 2018 An effective cryostat design of conduction-cooled HTS magnets for a 300-kW-class superconducting induction heater *IEEE Trans. Appl. Supercond.* **28** 4601705
- [16] Hahn S *et al* 2019 45.5-tesla direct-current magnetic field generated with a high-temperature superconducting magnet *Nature* **570** 496–9
- [17] Wang X, Hahn S, Kim Y, Bascuñán J, Voccio J, Lee H G and Iwasa Y 2012 Turn-to-turn contact characteristics for an equivalent circuit model of no-insulation REBCO pancake coil *Supercond. Sci. Technol.* **26** 035012
- [18] Bhattarai K R, Kim K, Kim S, Lee S G and Hahn S 2017 Quench analysis of a multiwidth no-insulation 7-T 78-mm REBCO magnet *IEEE Trans. Appl. Supercond.* **27** 4603505
- [19] Yang D G, Song J B, Choi Y H, Kim S G, Choi Y S and Lee H 2017 A study on electrical characteristics of multilayered metallic-insulation coils *IEEE Trans. Appl. Supercond.* **27** 7700206
- [20] Yanagisawa Y, Sato K, Yanagisawa K, Nakagome H, Jina X, Takahashi M and Maeda H 2014 Basic mechanism of self-healing from thermal runaway from uninsulated REBCO pancake coils *Physica C* **499** 40–4
- [21] Markiewicz W D, Jaroszynski J J, Abraimov D V, Joyner R E and Khan A 2016 Quench analysis of pancake wound REBCO coils with low resistance between turns *Supercond. Sci. Technol.* **29** 025001
- [22] Song H and Wang Y 2015 Simulations of nonuniform behaviors of multiple no-insulation (RE)Ba<sub>2</sub>Cu<sub>3</sub>O<sub>7-x</sub> HTS pancake coils during charging and discharging *IEEE Trans. Appl. Supercond.* **26** 4700105
- [23] Song J-B, Hahn S, Lecrevisse T, Voccio J, Bascuñán J and Iwasa Y 2015 Over-current quench test and self-protecting behavior of a 7 T/78 mm multi-width no-insulation REBCO magnet at 4.2 K *Supercond. Sci. Technol.* **28** 114001
- [24] Wang T, Noguchi S, Wang X, Arakawa I, Minami K, Monma K, Ishiyama A, Hahn S and Iwasa Y 2015 Analyses of transient behaviors of no-insulation REBCO pancake coils during sudden discharging and overcurrent *IEEE Trans. Appl. Supercond.* **25** 4603409
- [25] Ikeda A, Oki T, Wang T, Ishiyama A, Monma K, Noguchi S, Watanabe T and Nagaya S 2016 Transient behaviors of no-insulation REBCO pancake coil during local normal-state transition *IEEE Trans. Appl. Supercond.* **26** 4600204
- [26] Wang Y, Chan W K and Schwartz J 2016 Self-protection mechanisms in no-insulation (RE)Ba<sub>2</sub>Cu<sub>3</sub>O<sub>x</sub> high temperature superconductor pancake coils *Supercond. Sci. Technol.* **29** 045007
- [27] Wang Y, Zhang M, Yuan W, Hong Z, Jin Z and Song H 2017 Non-uniform ramping losses and thermal optimization with turn-to-turn resistivity grading in a (RE)Ba<sub>2</sub>Cu<sub>3</sub>O<sub>x</sub> magnet consisting of multiple no-insulation pancake coils *J. Appl. Phys.* **122** 053902
- [28] Liu D, Zhang W, Yong H and Zhou Y 2018 Thermal stability and mechanical behavior in no-insulation high-temperature superconducting pancake coils *Supercond. Sci. Technol.* **31** 085010
- [29] Miyao R, Igarashi H, Ishiyama A and Noguchi S 2017 Thermal and electromagnetic simulation of multi-stacked no-insulation REBCO pancake coils on normal-state transition by PEEC model *IEEE Trans. Appl. Supercond.* **28** 4601406

- [30] Garrett M W 1963 Calculation of fields, forces, and mutual inductances of current systems by elliptic integrals *J. Appl. Phys.* **34** 2567
- [31] Thieme C L H, Gagnon K J, Coulter J Y, Song H and Schwartz J 2009 Stability of second generation HTS pancake coils at 4.2 K for high heat flux applications *IEEE Trans. Appl. Supercond.* **19** 1626
- [32] Hilton D K, Gaverlin A V and Trociewitz U P 2015 Practical fit functions for transport critical current versus field magnitude and angle data from (RE)BCO coated conductors at fixed low temperatures and in high magnetic fields *Supercon. Sci. Technol.* **28** 074002
- [33] Senatore C, Barth C, Bonura M, Kulich M and Mondonico G 2015 Field and temperature scaling of the critical current density in commercial REBCO coated conductors *Supercon. Sci. Technol.* **29** 014002
- [34] Iwasa Y 2009 *Case Studies in Superconducting Magnets* (New York: Springer) (<https://doi.org/10.1007/b112047>)
- [35] Gyuraki R, Benkel T, Schreiner F, Sirois F and Grilli F 2019 Fluorescent thermal imaging of a non-insulated pancake coil wound from high temperature superconductor tape *Supercond. Sci. Technol.* **32** 105006
- [36] Bobrov E S and Williams J E C 1980 Stresses in superconducting solenoids *Mechanics of Superconducting Structures* **41** 13–41
- [37] Lu J, Goddard R, Han K and Hahn S 2017 Contact resistance between two REBCO tape under load and load cycles *Supercond. Sci. Technol.* **30** 045005
- [38] Noguchi S, Kim K and Hahn S 2018 Simulation on electrical field generation by hall effect in no-insulation REBCO pancake coils *IEEE Trans. Appl. Supercond.* **28** 4901805
- [39] Michael P C, Park D, Choi Y H, Lee J, Li Y, Bascañán J, Noguchi S, Hahn S and Iwasa Y 2019 Assembly and Test of a 3-Nested-Coil 800-MHz REBCO Insert (H800) for the MIT 1.3 GHz LTS/HTS NMR Magnet *IEEE Trans. Appl. Supercond.* **29** 4300706
- [40] Park D, Bascañán J, Michael P C, Lee J, Hyuck Choi Y, Li Y, Hahn S and Iwasa Y 2019 MIT 1.3-GHz LTS/HTS NMR magnet: post quench analysis and new 800-MHz insert design *IEEE Trans. Appl. Supercond.* **29** 4300804
- [41] Noguchi S, Park D, Choi Y, Lee J, Li Y, Michael P C, Bascañán J, Hahn S and Iwasa Y 2019 Quench analyses of the MIT 1.3-GHz LTS/HTS NMR magnet *IEEE Trans. Appl. Supercond.* **29** 4301005